



ELSEVIER

Available online at www.sciencedirect.com

SCIENCE @ DIRECT®

Journal of Sound and Vibration 281 (2005) 995–1021

JOURNAL OF
SOUND AND
VIBRATION

www.elsevier.com/locate/jsvi

Effect of nonlinear impact damping on the frequency response of a torsional system with clearance

T.C. Kim, T.E. Rook, R. Singh*

Acoustics and Dynamics Laboratory, Department of Mechanical Engineering and The Center for Automotive Research, The Ohio State University, 650 Ackerman Road, Columbus, OH 43202, USA

Received 4 March 2003; accepted 10 February 2004

Available online 14 October 2004

Abstract

In this article we examine a particular nonlinear impact damping model that has been well accepted by the scientific community. First, we consider the damping element with a linear spring and examine the nonlinear frequency response characteristics of a torsional system. Second, the impact damping is examined along with the clearance nonlinearity including the backlash problem. Three semi-analytical methods, namely the Describing Function Method, Multi-term Harmonic Balance Method and Stochastic Linearization Method, are utilized to investigate the effect of impact damping. Feasibility of such methods is confirmed by comparing predictions with results yielded by a numerical method. The differences between impact damping and linear viscous damping mechanism are studied in terms of frequency responses, time histories, and the minimum number of harmonics required to simulate the behavior given sinusoidal excitations. Furthermore, the effect of impact damping on sub- and super-harmonic responses and quasi-periodic regimes are examined.

© 2004 Elsevier Ltd. All rights reserved.

1. Introduction

Hunt and Crossley [1] proposed a nonlinear damping model when compact solid bodies impact each other. Essentially, they reinterpreted the classical model of the coefficient of restitution, and

*Corresponding author. Tel.: +1-614-292-9044; fax: +1-614-292-3163.

E-mail address: singh.3@osu.edu (R. Singh).

Nomenclature		
		ϕ phase angle (rad)
		$\theta, \dot{\theta}, \ddot{\theta}$ absolute displacement, velocity and acceleration (rad, rad/s, rad/s ²)
a	Fourier transformed relative displacement δ	σ smoothing factor
b	break points for stages in a clearance nonlinearity (rad)	τ period (s)
C	viscous damping coefficient (Nm s)	Ω non-dimensional frequency ($\Omega = \omega_p/\omega_r$)
\bar{C}	equivalent viscous damping (1/s)	$\bar{\Omega}_{p1}$ non-dimensional primary harmonic corresponding to stiffness of stage 1
c	Fourier components of nonlinear function in HBM	ω angular velocity (rad/s)
$E[\]$	expectation operator	Ξ derivative of DFT matrix
F	effective external torque (Nm/kg m ²)	Ψ spectral time toward transition points
f_δ	instantaneous stiffness vector of nonlinear function	ζ damping ratio
$f(\)$	nonlinear function (rad)	\mathfrak{F} Fourier transform
$g(\)$	linearized nonlinear function (rad)	
$\hat{g}(\)$	smoothened form of sgn function	
G	simplification function in DFM coefficient calculation	<i>Subscripts</i>
H	simplification function in DFM coefficient calculation	– column vector
I	effective torsional moment of inertia (kg m ²)	= matrix
I_i	torsional moment of inertia (kg m ²)	1,2,3,... stiffness or damping stages, element index
J	Jacobian matrix	C_i clutch stages
ℓ	separation distance between primary harmonic and mean operation point	e external excitation
K	contact stiffness (Nm/rad)	ef effective term
\bar{K}	equivalent stiffness (dimensionless)	G impact pair
N	sampling points per cycle in HBM	IMP impact related
N_f	DFM coefficient	j torque harmonic index
n	harmonic index used in HBM	m mean component
q	Hertzian compliance exponent	max maximum limit
R	residual in frequency domain	min minimum limit
r	residual in time domain	p alternating or perturbation component
T	torque (Nm)	r resonance
t	time (s)	rms root-mean-square value
		S stiffness-related term
<i>Greeks</i>		<i>Superscripts</i>
α	stiffness of first stage	\cdot first derivative with respect to time (velocity)
β	impact damping coefficient (s/rad)	$\cdot\cdot$ second derivative with respect to time (acceleration)
$\delta, \dot{\delta}, \ddot{\delta}$	relative displacement, velocity and acceleration (rad, rad/s, rad/s ²)	– non-dimensional value when placed over a variable
Γ	DFT matrix	+ pseudo-inverse of matrix
Φ	time scaling ($\Phi = \omega t + \phi$)	T transpose of matrix
		–1 inverse of matrix

Abbreviations		NSU	numerical simulation (up frequency sweep)
DFT	discrete Fourier transform	NSD	numerical simulation (down frequency sweep)
HBM	harmonic balance method	SDOF	single-degree-of-freedom
MDOF	multi-degree-of-freedom	SLM	stochastic linearization method
NS	numerical simulation (Runge–Kutta 4(5))		

suggested damping force or torque be described as $\beta K \delta^q \dot{\delta}$ where β is the impact damping coefficient, K is the contact stiffness, δ is the dynamic displacement, $\dot{\delta}$ is the velocity, and q is the Hertzian compliance exponent. In particular, this model removed the non-physical artifact associated with a linear model that assumes the $C\dot{\delta}$ from where C is the viscous damping coefficient as utilized earlier by Dubowsky and Freudenstein [2,3]. Subsequent investigators [4–8] have employed the nonlinear impact damping model where C could be defined in terms of $\beta K \delta^q$. Veluswami et al. [4,5], Azar and Crossley [6], and Padmanabhan and Singh [8] have reported reasonable agreements between simulations based on the nonlinear impact damping model and experiments.

In this article, we examine the effect of Hunt and Crossley's impact damping model (with $q=1$) on the nonlinear frequency response characteristics of a torsional system with clearance nonlinearity as depicted in Fig. 1. The physical system is under the influence of a mean load and is subject to harmonic excitation. This particular issue was earlier examined by Padmanabhan and Singh [8]. They along with Herbert and McWhannell [9] found significant changes in frequency responses when the nonlinear impact damping term was included. Yet, the characteristics of impact damping itself, without the influence of clearance-type nonlinearity, were not studied. Furthermore, super- and sub-harmonics have not been studied for this type of system before.

Torsional systems with clearances have mostly been examined with viscous or fluid-induced drag damping elements [1–3,8]. Both digital and analog simulations have been successfully utilized [10–21]. Also, semi-analytical techniques have been used to construct the nonlinear frequency responses [13–21]. Refer to Kim et al. [20,21], Comparin and Singh [12,13], and Rook and Singh [19] for a comprehensive review of the methods employed earlier. In this article, we will be employing several semi-analytical techniques to examine the nonlinear characteristics of impact damping, with and without the clearance nonlinearity.

2. Problem formulation

2.1. Torsional sub-system

Vehicle drivetrains and other torsional systems often contain multi-staged clutches and at least one gear pair with backlash [11–21]. Dual-mass flywheel or spline/synchronizer with clearances may also be found in practice [22,23]. One could decompose such practical systems in terms of coupled torsional sub-systems, each containing one clearance-type nonlinear stiffness as given by

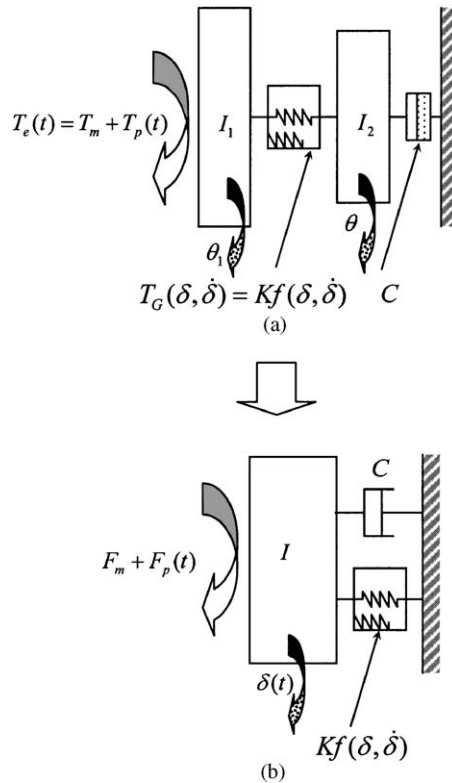


Fig. 1. Torsional sub-system with clearance nonlinearity $f(\delta, \dot{\delta})$. (a) Two degree-of-freedom semi-definite system; and (b) single degree-of-freedom definite system when $\delta = \theta_1 - \theta_2$.

function $f(\delta, \dot{\delta})$ where δ and $\dot{\delta}$ are the relative displacement and velocity, respectively, as shown in Fig. 1. Here, piecewise linear or nonlinear restoring force (torque) characteristics may be employed.

The excitation torque $T_e(t)$, say from an internal combustion engine, fluctuates significantly between low (around the compression stage) and high (around the ignition stage) values. Therefore, the $T_e(t)$ can be decomposed into mean T_m and perturbation $T_p(t)$ parts. Also, one must note that the relationship between the crankshaft rotational frequency ω_e and the fundamental excitation frequency (firing frequency) ω_p of $T_p(t)$. It depends on type of the engine, number of cylinders and crankshaft configuration. For example, $\omega_p = 2\omega_e$ for an I-4 engine with 180° crankshaft configuration. $T_e(t)$ is expanded via Fourier series:

$$T_e(t) = T_m + \sum_{j=1}^{\infty} T_{pj} \sin(j\omega_p t + \phi_j) \quad \text{or} \quad T_e(t) = T_m + \sum_{j=1}^{\infty} T_{pj} \cos(j\omega_p t + \phi_j). \quad (1)$$

Here, j represents the torque harmonic (order) index, and the mean term $T_m = E[\tilde{T}_e(t)]$, where $E[\]$ is the expectation operator.

The coupled equations for the semi-definite torsional system of Fig. 1(a) can be reduced to a single equation for the equivalent SDOF system of Fig. 1(b) where $\delta = \theta_1 - \theta_2$.

$$\ddot{\delta} + \frac{C}{I} \dot{\delta} + T_G(\delta, \dot{\delta}) = F(t), \quad T_G(\delta, \dot{\delta}) = Kf(\delta, \dot{\delta}), \tag{2a,b}$$

$$F(t) = F_m + \sum_{j=1}^{\infty} F_{pj} \sin(j\omega_p t + \phi_j). \tag{2c}$$

Here, $I = I_1 I_2 / (I_1 + I_2)$ is the effective torsional inertia, $F_m = T_m / I$ is the effective mean torque, T_G is the constraining torque, K is the contact stiffness, and $F_{pj} = T_{pj} / I_1$ is the effective amplitude for the j th harmonic of pulsating torque. A viscous damping term (C) is included so that it may describe the fluid-induced damping in drivetrains. Note that T_G is in the units of Nm, $f(\delta, \dot{\delta})$ is in rad, and K is in Nm/rad.

2.2. Clearance and impact damping nonlinearities

Nonlinear elastic torque $T_G = Kf(\delta, \dot{\delta})$ relationship for a torsional system with clearance and impact damping nonlinearities is described in Fig. 2(a). Here, I is viewed as rigid mass oscillating between two perfectly elastic walls with clearance $\pm b$. We express the nonlinear stiffness function

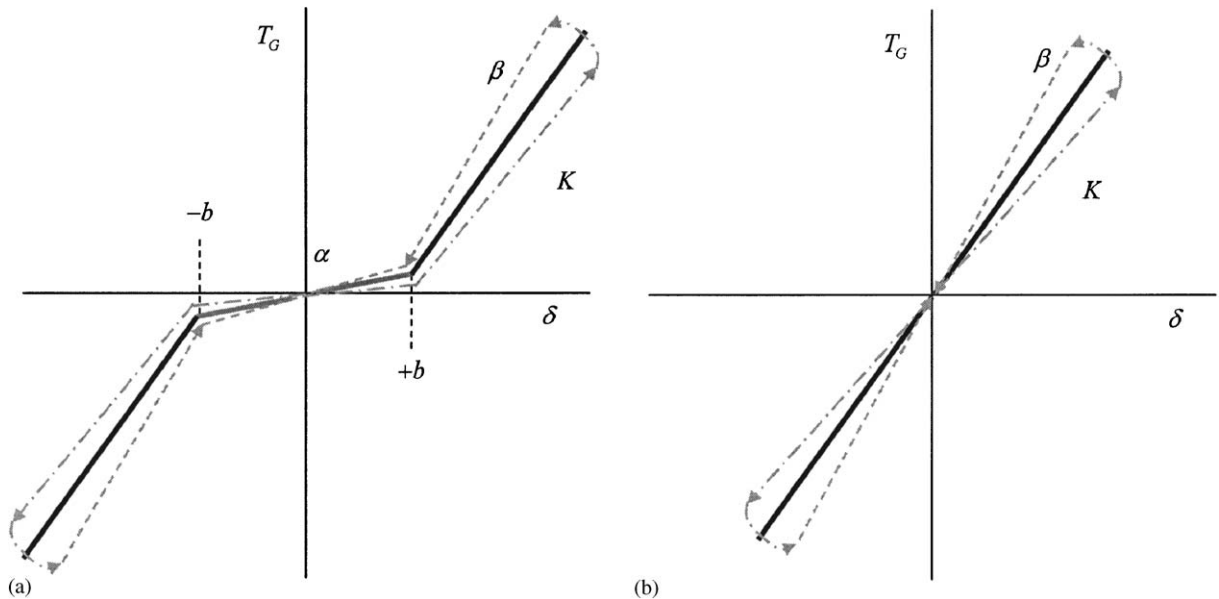


Fig. 2. Illustration of clearance and impact damping nonlinearities. (a) Dual-staged stiffness with impact damping; and (b) impact damping alone.

$f_S(\delta)$ for the dual-staged curve of Fig. 2(a) (with stiffnesses α and 1) as

$$f_S(\delta) = \begin{cases} \delta - (1 - \alpha)b, & b < \delta \\ \alpha\delta, & -b \leq \delta \leq b \\ \delta + (1 - \alpha)b, & \delta < -b \end{cases} \\ = \delta + (1 - \alpha) \frac{\text{abs}(\delta - b) - \text{abs}(\delta + b)}{2}. \quad (3)$$

Next we define the impact damping function $f_{\text{IMP}}(\delta, \dot{\delta})$ where β is the impact damping coefficient; note that β is in s/rad:

$$f_{\text{IMP}}(\delta, \dot{\delta}) = f_S(\delta)\beta\dot{\delta}. \quad (4)$$

Therefore, the combined nonlinear function $f(\delta, \dot{\delta})$ which includes $f_S(\delta)$ and the impact damping element is described as

$$f(\delta, \dot{\delta}) = \begin{cases} (\delta - (1 - \alpha)b)(1 + \beta\dot{\delta}), & b < \delta \\ \alpha\delta(1 + \beta\dot{\delta}), & -b \leq \delta \leq b \\ (\delta + (1 - \alpha)b)(1 + \beta\dot{\delta}), & \delta < -b \end{cases} \\ = \left(\delta + (1 - \alpha) \frac{\text{abs}(\delta - b) - \text{abs}(\delta + b)}{2} \right) (1 + \beta\dot{\delta}). \quad (5)$$

The backlash b is defined in angular terms (deg) along the line of action. When I_1 and I_2 move towards each other, $\dot{\delta} > 0$ and the contact regime experiences elastic deformation according to β and T_G follows the lower locus (dash-dot line) in Fig. 2(b). Likewise, when $\dot{\delta} < 0$, I_1 and I_2 rebound and T_G follows the upper locus (dashed line). A thin oil film between the gap generates the near-zero first stage stiffness, $\alpha \approx 0$, within the initial displacement of $-b < \delta < b$. When δ is larger than $\pm b$, T_G is governed by K .

Finally, consider a special case of the above, when there is no backlash, i.e. $b = 0$. This condition simulates a purely linear stiffness case with nonlinear impact damping as shown in Fig. 2(b). As described by Hunt and Crossley [1], the gear teeth (being in compressive contact) impact microscopically between the elastic deformations and thereby absorb a small amount of energy. Note that in this condition, there is a sign change at $b = 0$ as shown in Fig. 2(b). Eq. (5) for this case is simplified as

$$f(\delta, \dot{\delta}) = \delta(1 + \beta\dot{\delta}). \quad (6)$$

2.3. Analytical and numerical methods

Several semi-analytical techniques will be employed to construct the nonlinear frequency response characteristics of a system with clearance and impact damping. First, impact damping formulation will be included in the describing function method (DFM) [24,25] that was introduced by Comparin and Singh [12,13] for a vibro-impact pair. Second, we will also extend the work of Padmanabhan and Singh [8] and Rook and Singh [19] who investigated both time and frequency domain characteristics of clearance nonlinearities based on the application of harmonic

balance method (HBM). Third, we will apply the concept of equivalent stiffness based on the stochastic linearization method (SLM) as proposed earlier by Rook and Singh [19]. This would allow us to determine the spectrally varying viscous damping and stiffness values. Fourth, we will employ the multi-HBM that was recently described in our articles [20,21]. We will utilize it to compare predictions based on DFM and SLM. Results will also be compared with those obtained using numerical (digital) simulations (NI) based on the modified Runge–Kutta 5(4) integration technique due to Dormand and Prince [26], which has been found to be reliable by Padmanabhan and Singh [8].

Simple analytical predictions regarding the impact damping itself (without the contaminating influence of clearance nonlinearity) will be introduced. Two cases of α are considered when both nonlinear damping and clearance functions are included: (1) $\alpha=0$ (gear backlash problem), and (2) $0 < \alpha < 0.25$ (a strong nonlinearity seen in clutches). In particular, we focus attention on super- and sub-harmonics and explore some issues that were not fully resolved by Comparin and Singh [12,13] and Padmanabhan and Singh [8]. For instance, we calculate equivalent viscous damping and stiffness values corresponding to impact damping and clearance. The effect of impact damping on quasi-periodic or chaotic response regimes is briefly examined as well. Finally, semi-analytical methods will be evaluated by comparing time or frequency domain predictions with those yielded by digital simulations [8,18,19,21].

3. Describing function method (DFM)

3.1. Formulation

The steady-state solution $\delta(t) = \delta(t + \tau_p)$ of Eq. (2) is assumed to be periodic (with $\tau_p = 2\pi/\omega_p$) in order to find the Fourier series approximation of nonlinear functions [19–25]. The periodic forms of the assumed excitation $F(t)$ and response $\delta(t)$ are reduced to sinusoidal waveforms of frequency ω_p as

$$F(t + \tau_p) = F_m + \sum_{j=1}^{\infty} F_{pj} \sin(j\omega_p t + \phi_{ej}) \cong F_m + F_{p1} \sin(\omega_p t + \phi_{e1}), \tag{7}$$

$$\delta(t + \tau_p) = \delta_m + \sum_{j=1}^{\infty} \delta_{pj} \sin(j\omega_p t + \phi_j) \cong \delta_m + \delta_{p1} \sin(\omega_p t + \phi_1). \tag{8}$$

Expand $f(\delta, \dot{\delta})$ of Eq. (5) with only the primary harmonic ($j=1$) as follows where Φ_p is defined as $\Phi_p = \omega_p t + \phi_{e1}$, and N_{fm} , N_{fp1} and N_{fp2} are the describing functions or coefficients:

$$f(\delta, \dot{\delta}) \cong N_{fm}\delta_m + N_{fp1}\delta_{p1} \sin \Phi_p + N_{fp2}\delta_{p1} \cos \Phi_p. \tag{9}$$

First, write the harmonic solution as follows where the natural frequency $\omega_r = \sqrt{K/I}$ of corresponding linear system is introduced:

$$-\omega_p^2 \delta_{p1} \sin(\Phi_p) + \frac{C}{I} \omega_p \delta_{p1} \cos(\Phi_p) + \omega_r^2 (N_{fm}\delta_m + N_{fp1}\delta_{p1} \sin(\Phi_p) + N_{fp2}\delta_{p1} \cos(\Phi_p)) = F_m + F_{p1} \sin(\omega_p t + \phi_{e1}). \tag{10}$$

Second, define the describing functions N_{fm} , N_{fp1} and N_{fp2} as

$$N_{fm}(\delta_m, \delta_{p1}) = \frac{1}{2\pi\delta_m} \int_0^{\tau_p} f(\delta, \dot{\delta}) d\Phi_p, \quad N_{fp1}(\delta_m, \delta_{p1}) = \frac{1}{\pi\delta_p} \int_0^{\tau_p} f(\delta, \dot{\delta}) \sin \Phi_p d\Phi_p, \quad (11a,b)$$

$$N_{fp2}(\delta_m, \delta_{p1}) = \frac{1}{\pi\delta_p} \int_0^{\tau_p} f(\delta, \dot{\delta}) \cos \Phi_p d\Phi_p. \quad (11c)$$

Once the Fourier series expansions for $f(\delta, \dot{\delta})$ are developed, they are substituted into the original differential equation along with the assumed forms of solution and excitation [24,25]. The coefficients of like harmonics are equated to yield a set of nonlinear-coupled algebraic equations in terms of unknown amplitudes and phases. The bias or mean (with subscript m) term is given by the following where N_{fm} is a function of both δ_m and δ_{p1} :

$$\omega_r^2 N_{fm}(\delta_m, \delta_{p1}) \delta_m = F_m. \quad (12a)$$

The response at the primary harmonic of ω_p is given by $\sin(\Phi_p)$ and $\cos(\Phi_p)$ terms as

$$(-\omega_p^2 + \omega_r^2 N_{fp1}(\delta_m, \delta_{p1})) \delta_{p1} = F_{p1} \sin(\phi_{e1} - \phi_1), \quad (12b)$$

$$\left(\frac{C}{I} \omega_p + \omega_r^2 N_{fp2}(\delta_m, \delta_{p1}) \right) \delta_{p1} = F_{p1} \cos(\phi_{e1} - \phi_1). \quad (12c)$$

Since the above equations are nonlinear algebraic equations with two unknowns, δ_m and δ_{p1} , we prepare to solve them using the Newton–Raphson method. Therefore, the desired solutions can be written in the following form. These represent the nonlinear frequency response characteristics:

$$\delta_m = F_m / (\omega_r^2 N_{fm}), \quad \delta_{p1} = F_{p1} / \sqrt{(-\omega_p^2 + \omega_r^2 N_{fp1})^2 + \left(\frac{C}{I} \omega_p + \omega_r^2 N_{fp2} \right)^2}, \quad (13a,b)$$

$$\phi_1 = \tan^{-1} \left(\frac{-\omega_p^2 + \omega_r^2 N_{fp1}}{(C/I)\omega_p + \omega_r^2 N_{fp2}} \right) + \phi_{e1}. \quad (13c)$$

3.2. Fourier coefficients for impact damping alone

Now, we consider Eq. (6), with only impact damping nonlinearity. The DFM coefficients of Eq. (11) are evaluated over a period $\tau_p = 2\pi$:

$$N_{fm}(\delta_m, \delta_{p1}) = \frac{1}{2\pi\delta_m} \int_0^{2\pi} \delta(1 + \beta\dot{\delta}) d\Phi_p = 1, \quad (14a)$$

$$N_{fp1}(\delta_m, \delta_{p1}) = \frac{1}{\pi\delta_p} \int_0^{2\pi} \delta(1 + \beta\dot{\delta}) \sin \Phi_p d\Phi_p = 1, \quad (14b)$$

$$N_{fp2}(\delta_m, \delta_{p1}) = \frac{1}{\pi\delta_p} \int_0^{2\pi} \delta(1 + \beta\dot{\delta}) \cos \Phi_p d\Phi_p = \delta_m \omega_p \beta. \quad (14c)$$

Thus, we find that the impact damping affects only the N_{fp2} term, and the mean and effective stiffness terms are not influenced. Therefore, δ_m , δ_{p1} , and ϕ_1 can be written as below when the viscous damping coefficient is ignored, and the excitation phase angle ϕ_{e1} is assumed to be equal to 0:

$$\delta_m = F_m/\omega_r^2, \quad \delta_{p1} = F_{p1}/\sqrt{(-\omega_p^2 + \omega_r^2)^2 + (\omega_r^2\delta_m\omega_p\beta)^2}, \tag{15a,b}$$

$$\phi_1 = \tan^{-1} \left(\frac{(-\omega_p^2 + \omega_r^2)}{(\omega_r^2\delta_m\omega_p\beta)} \right). \tag{15c}$$

3.3. Fourier coefficients for combined nonlinearities

For the case when clearance-type nonlinearity is combined with impact damping, the integrals of Eq. (11) are very difficult to evaluate. In general, we define three possible impact conditions; no impact, single-sided impact, and double-sided impact [12,13]. For the sake of illustration, consider the nonlinear function $f(\delta, \dot{\delta})$ of a backlash problem (with $\alpha=0$) with impact damping as

$$f(\delta, \dot{\delta}) = \begin{cases} (\delta - b)(1 + \beta\dot{\delta}), & \delta > b, \\ 0, & -b \leq \delta \leq b, \\ (\delta + b)(1 + \beta\dot{\delta}), & \delta < -b. \end{cases} \tag{16}$$

For the no impact case, Eqs. (14a–c) represent the DFM coefficients. Next, consider the single-sided impact case when the mean operating point is in the second stage ($\delta_m > b$), and impact condition is guided by: $\delta_m - b \leq \delta_{p1} < \delta_m + 2b$. Define, $\psi_1 = \arcsin(\delta_m - b)/\delta_{p1}$ and $\psi_2 = \arcsin(\delta_m + 2b)/\delta_{p1}$ as the corresponding spatial “times” to reach the transition points b and $-b$. One must note that even finding exact value of ψ_1 and ψ_2 are impossible when multi-harmonic terms are involved. The DFM coefficients for the fundamental harmonic only case are formulated as

$$N_{fm}(\delta, \dot{\delta}) = \frac{1}{2\pi\delta_m} \left\{ \int_0^{\pi+\psi_1} (\delta - b)(1 + \beta\dot{\delta}) d\Phi + \int_{2\pi-\psi_1}^{2\pi} (\delta - b)(1 + \beta\dot{\delta}) d\Phi \right\}, \tag{17a}$$

$$N_{fp1}(\delta, \dot{\delta}) = \frac{1}{\pi\delta_{p1}} \left\{ \int_0^{\pi+\psi_1} (\delta - b)(1 + \beta\dot{\delta}) \sin \Phi d\Phi + \int_{2\pi-\psi_1}^{2\pi} (\delta - b)(1 + \beta\dot{\delta}) \sin \Phi d\Phi \right\}, \tag{17b}$$

$$N_{fp2}(\delta, \dot{\delta}) = \frac{1}{\pi\delta_{p1}} \left\{ \int_0^{\pi+\psi_1} (\delta - b)(1 + \beta\dot{\delta}) \cos \Phi d\Phi + \int_{2\pi-\psi_1}^{2\pi} (\delta - b)(1 + \beta\dot{\delta}) \cos \Phi d\Phi \right\}. \tag{17c}$$

For the double-sided impact case ($\delta_{p1} > \delta_m + 2b$) given the mean operating point is in the second stage ($\delta_m > b$), express the DFM coefficients as follows:

$$N_{fm} = \frac{1}{2\pi\delta_m} \left\{ \int_0^{\pi+\psi_1} (\delta - b)(1 + \beta\dot{\delta}) d\Phi + \int_{\pi+\psi_2}^{2\pi-\psi_2} (\delta + b)(1 + \beta\dot{\delta}) d\Phi + \int_{2\pi-\psi_1}^{2\pi} (\delta - b)(1 + \beta\dot{\delta}) d\Phi \right\}, \quad (18a)$$

$$N_{fp1} = \frac{1}{\pi\delta_{p1}} \left\{ \int_0^{\pi+\psi_1} (\delta - b)(1 + \beta\dot{\delta}) \sin \Phi d\Phi + \int_{\pi+\psi_2}^{2\pi-\psi_2} (\delta + b)(1 + \beta\dot{\delta}) \sin \Phi d\Phi + \int_{2\pi-\psi_1}^{2\pi} (\delta - b)(1 + \beta\dot{\delta}) \sin \Phi d\Phi \right\}, \quad (18b)$$

$$N_{fp2} = \frac{1}{\pi\delta_{p1}} \left\{ \int_0^{\pi+\psi_1} (\delta - b)(1 + \beta\dot{\delta}) \cos \Phi d\Phi + \int_{\pi+\psi_2}^{2\pi-\psi_2} (\delta + b)(1 + \beta\dot{\delta}) \cos \Phi d\Phi + \int_{2\pi-\psi_1}^{2\pi} (\delta - b)(1 + \beta\dot{\delta}) \cos \Phi d\Phi \right\}. \quad (18c)$$

Even though Eqs. (17a–c) and (18a–c) look complicated, we have found that the nonlinear impact damping element affects only the N_{fp2} term as summarized in Table 1. Like Eqs. (14a–c), this term is found to be proportion of $\beta\omega_p\delta_m$ with some δ_p influence. The N_{fm} and N_{fp1} terms only depend on clearance-type nonlinearity since they are free from the influence of the impact damping term β . The N_{fm} and N_{fp1} terms range between 0 and 1 according to the three impact conditions. When the system stays dominantly in $\alpha = 0$ (backlash) regime, the Fourier coefficients have lower values. Refer to Comparin and Singh [12,13] for results on the clearance nonlinearity alone. Overall, we observe that the nonlinear response seems to be more governed by the clearance and less by the impact damping.

4. Stochastic linearization method (SLM)

4.1. Fourier coefficients for combined nonlinearity

This SLM is developed from the “effective stiffness concept” that was introduced by Rook and Singh [19] to qualitatively understand the impact behavior of a clearance nonlinearity, based on the concept given by Wallaschek [27]. In this article, we employ this concept to find the effective

Table 1
Describing function coefficients of a clearance with impact damping

(a) *Single-sided impact case*

$$N_{fm}(\delta, \dot{\delta}) = \frac{1}{2\pi\delta_m} ((\pi + 2\Psi_1)\delta_m + 2G\delta_{p1} - (\pi + 2\Psi_1)b)$$

$$N_{fp1}(\delta, \dot{\delta}) = \frac{1}{2\pi\delta_{p1}} ((2\delta_m G + (\pi + 2\Psi_1)\delta_{p1} - 2Gb)$$

$$N_{fp2}(\delta, \dot{\delta}) = \frac{\beta\omega_p}{6\pi\delta_{p1}} (3\pi\delta_m\delta_p + 2G\delta_m^2 - 4bG\delta_m - 3\pi b\delta_p - 6b\Psi_1\delta_p + 4G\delta_p^2 + 2b^2G + 6\delta_m\delta_p\Psi_1)$$

(b) *Double-sided impact case*

$$N_{fm}(\delta, \dot{\delta}) = \frac{1}{\pi\delta_m} ((\pi + \Psi_1 - \Psi_2)\delta_m + (G - H)\delta_{p1} - (\Psi_1 + \Psi_2)b)$$

$$N_{fp1}(\delta, \dot{\delta}) = \frac{1}{\pi\delta_{p1}} ((G - H)\delta_m + (\pi + \Psi_1 - \Psi_2)\delta_{p1} - Gb)$$

$$N_{fp2}(\delta, \dot{\delta}) = \frac{\beta\omega_p}{3\pi\delta_{p1}} ((G - H)\delta_m^2 + (\pi + \Psi_1 - \Psi_2)3\delta_m\delta_p + (G - 2H)b^2 + 2(G - H)\delta_p^2 - (2G - H)\delta_m b - 3b\delta_p(\Psi_1 + \Psi_2))$$

$$\Psi_1 = \arcsin \frac{\delta_m - b}{\delta_{p1}}, \quad \Psi_2 = \arcsin \frac{\delta_m + 2b}{\delta_{p1}}$$

$$G = \sqrt{\frac{\delta_{p1}^2 - \delta_m^2 + 2\delta_m b - b^2}{\delta_{p1}^2}}$$

$$H = \sqrt{\frac{\delta_{p1}^2 - \delta_m^2 - 4\delta_m b - 4b^2}{\delta_{p1}^2}}$$

viscous damping as well as stiffness values. For example, the nonlinear function $f(\delta, \dot{\delta})$ in rad is estimated by a linear model $g(\delta, \dot{\delta}) = \overline{C}\dot{\delta} + \overline{K}\delta$, and the error between these two functions is minimized in the least squares sense. Here, effective viscous damping coefficient \overline{C} is in s, and the effective stiffness coefficient \overline{K} is dimensionless. Since we assume the response of $\delta(t)$ to be periodic, only the ergodic data which provide the relationships $\langle \delta\dot{\delta} \rangle = 0$ and $\langle \delta\ddot{\delta} \rangle = 0$ are used in

subsequent analysis. Then the following equations for effective terms must be satisfied at any ω_p :

$$\overline{K}(\omega_p) = \frac{\langle f(\delta, \dot{\delta})\delta \rangle - \langle f(\delta, \dot{\delta}) \rangle \langle \delta \rangle}{\langle \delta^2 \rangle - \langle \delta \rangle^2}, \quad \overline{C}(\omega_p) = \frac{\langle f(\delta, \dot{\delta})\dot{\delta} \rangle}{\langle \dot{\delta}^2 \rangle}, \tag{19a,b}$$

$$K_{ef}(\omega_p) = K\overline{K}(\omega_p), \quad C_{ef}(\omega_p) = K\overline{C}(\omega_p)I, \tag{19c,d}$$

where $\langle \cdot \rangle$ is the expectation operator or time domain average, and the units of C_{ef} are in Nm s/rad. For the effective viscous damping, the term $\langle f(\delta, \dot{\delta})\dot{\delta} \rangle$ represents the actual power dissipated. Thus the $\overline{C}(\dot{\delta}^2)$ term implies an equivalent but normalized dissipated power.

4.2. Effective terms for impact damping alone

Now, consider the case of the nonlinear impact damping only with $f(\delta, \dot{\delta}) = \delta(1 + \beta\dot{\delta})$. The effective stiffness is

$$\overline{K}(\omega_p) = \frac{\langle f\delta \rangle - \langle f \rangle \langle \delta \rangle}{\langle \delta^2 \rangle - \langle \delta \rangle^2} = \frac{\langle \delta^2 + \beta\delta^2\dot{\delta} \rangle - \langle \delta^2 \rangle - \beta\langle \delta\dot{\delta} \rangle}{\langle \delta^2 \rangle - \langle \delta \rangle^2} \tag{20}$$

and $\langle \delta\dot{\delta} \rangle = \langle d/dt(\frac{1}{2}\delta^2) \rangle = \frac{1}{2}d/dt\langle \delta^2 \rangle = 0$ since δ and $\dot{\delta}$ are orthogonal to each other and we are considering stationary responses. Then simplify the effective stiffness expression as

$$\overline{K}(\omega_p) = 1 + \beta \frac{\langle \delta^2\dot{\delta} \rangle}{\langle \delta^2 \rangle - \langle \delta \rangle^2}. \tag{21}$$

The term $\langle \delta^2\dot{\delta} \rangle$ can be calculated as below given the assumed solution as $\delta(t) = \delta_m + \delta_{p1} \sin(\Phi_p)$:

$$\begin{aligned} \langle \delta^2\dot{\delta} \rangle &= \left\langle \frac{d}{dt} \left(\frac{1}{3}\delta^3 \right) \right\rangle = \frac{1}{3} \frac{d}{dt} \langle \delta^3 \rangle \\ &= \int_0^{2\pi} (\delta_m + \delta_{p1} \sin(\Phi_p))^2 (\omega_p \delta_{p1} \cos(\Phi_p)) d\Phi_p = 0. \end{aligned} \tag{22}$$

Therefore, $K_{ef}(\omega_p) = 1$. The effective damping is calculated next as

$$\overline{C}(\omega_p) = \frac{\langle f\dot{\delta} \rangle}{\langle \dot{\delta}^2 \rangle} = \frac{\langle \delta\dot{\delta} \rangle + \beta\langle \delta\dot{\delta}^2 \rangle}{\langle \dot{\delta}^2 \rangle} = \delta_m\beta. \tag{23}$$

Here, $\langle \delta\dot{\delta} \rangle = 0$, and $\langle \delta\dot{\delta}^2 \rangle = \langle \delta \rangle \langle \dot{\delta}^2 \rangle$ owing to the fact that the covariance $\Sigma_{\delta\dot{\delta}^2}^2 = \langle \delta\dot{\delta}^2 \rangle - \langle \delta \rangle \langle \dot{\delta}^2 \rangle = 0$ because the two signals are uncorrelated. Therefore, $\langle \delta\dot{\delta}^2 \rangle = \int_0^{2\pi} (\delta_m + \delta_{p1} \sin \Phi) \times (\omega_p \delta_{p1} \cos \Phi)^2 d\Phi = \delta_m \omega_p^2 \delta_{p1}^2 \pi = \langle \delta \rangle \langle \dot{\delta}^2 \rangle$. Terms $\langle \delta \rangle = \delta_m$ and $\langle \dot{\delta}^2 \rangle = \int_0^{2\pi} (\delta_{p1} \cos(\Phi))^2 d\Phi = \omega_p^2 \delta_{p1}^2 \pi$.

5. Harmonic balance method (HBM)

As explained in our previous article [21], this method is essentially a form of Galerkin’s method based on the least squares fit in error reduction [28–35]. The residual or error $r(t)$ is the gap

between true input and estimated solutions, and it should go to zero for $\delta(t)$ when it satisfies the nonlinear differential equation. In the time domain, the *strong* form of residual is defined as

$$r(t) = T(t) - I\ddot{\delta} - C\dot{\delta} - Kf(\delta, \dot{\delta}) \rightarrow 0 \forall t. \tag{24}$$

Table 2
Parameters and excitations of a torsional sub-system

(a) <i>With impact damping alone</i>		
Case	Torque condition	Parameters and excitation
1	Large perturbation torque	$K = 1.0, I = 1.0, C = 1.0e - 6$
2	Small perturbation torque	$F_m = 0.25, F_p/F_m = 1.0, b = 0^\circ, \alpha = 1.0$
		$F_m = 0.10, F_p/F_m = 0.2, b = 0^\circ, \alpha = 1.0$
(b) <i>With impact damping and clearance nonlinearities</i>		
Case	Frequency response	Parameters and excitation
3	Super- and sub-harmonics	$K = 1.0, I = 1.0, C = 0.05$
4	Super-harmonics	$F_m = 0.25, F_p/F_m = 1.0, b = 1.0, \alpha = 0.15$
		$F_p = 0.01, F_p/F_m = 0.185, b = 10^\circ, \alpha = 0.00-0.15$

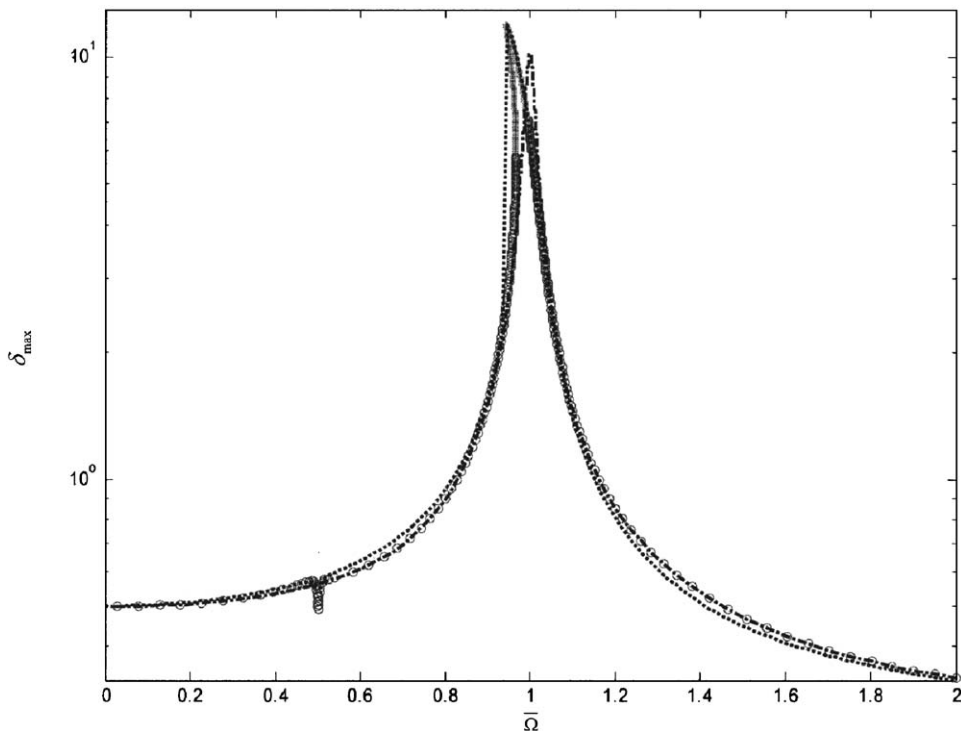


Fig. 3. Frequency response of nonlinear impact damping alone, for Case 1 of Table 2 when $\beta = 0.10$. Key: \circ , stable HBM ($n_{max} = 12$); $+$, unstable HBM; $- \cdot -$, DFM; and $\cdot \cdot \cdot$, NSD.

Here, $f(\delta, \dot{\delta})$ of Eq. (5) can be written as below after employing the “smoothening” function $\widehat{g}(\delta \mp b)$. The term σ is “smoothening factor” and the detailed explanations about $\widehat{g}(\delta \mp b)$ can be found in our previous article [21]

$$f(\delta, \dot{\delta}) = \left(\delta + (1 - \alpha) \frac{\widehat{g}(\delta - b) - \widehat{g}(\delta + b)}{2} \right) (1 + \beta \dot{\delta}), \tag{25a}$$

$$\widehat{g}(\delta \mp b) = (\delta \mp b) \tanh(\sigma(\delta \mp b)). \tag{25b}$$

Since input and response characteristics of a nonlinear system are assumed as periodic, frequency domain analysis can be applied by introducing the Fourier transformation (\mathfrak{F}) of both sides of Eq. (24). This yields the *weak* form residual (i.e. satisfied in only a least squares sense):

$$\mathfrak{R}(r(t)) = \underline{R} = \mathfrak{R}(T(t)) - I\mathfrak{R}(\ddot{\delta}) - C\mathfrak{R}(\dot{\delta}) - K\mathfrak{R}(f(\delta, \dot{\delta})) \rightarrow 0 \forall t. \tag{26}$$

Let the Fourier component vector of the sampled output be vector $\underline{a} = \mathfrak{R}(\delta(t))$, then the minimization of the residual in Newton–Raphson form is expressed as below. Finding a true \underline{a} is an iterative process using \underline{R}_0 , the residual from an initial guess, and the correction factor and $\Delta \underline{a}$, defined as $\Delta \underline{a} = -(\partial \underline{R} / \partial \underline{a})^{-1} \underline{R}$. Here, the term $\partial \underline{R} / \partial \underline{a}$ is the Jacobian matrix \underline{J} used in the Newton–Raphson corrector

$$\underline{J} = \frac{\partial \underline{R}}{\partial \underline{a}} = -\underline{I} \underline{\Xi}^2 - \underline{C} \underline{\Xi}^1 - \underline{K} \frac{\partial \underline{c}}{\partial \underline{a}}. \tag{27}$$

Now, the term $\partial \underline{c} / \partial \underline{a}$ is very difficult to calculate directly, and we choose to calculate the partial derivative of the nonlinearity in the time domain and convert it to the frequency domain [28–32]. As defined before, the Fourier components of the nonlinear function is vector $\underline{c} = \underline{\Gamma}^+ \underline{f}$ with $\underline{f} = \mathfrak{F}[f(\delta, \dot{\delta})]$, and amplitudes of each Fourier component of solution is vector $\underline{a} = \underline{\Gamma}^+ \underline{\delta}$. Here, matrix $\underline{\Gamma}^+$ is the pseudo-inverse of the DFT matrix $\underline{\Gamma}$ defined as $\underline{\Gamma}^+ = (\underline{\Gamma}^T \underline{\Gamma})^{-1} \underline{\Gamma}^T$. Now, rewrite the term $\partial \underline{c} / \partial \underline{a}$ as below since $\underline{\delta} = \underline{\Gamma} \underline{a} \rightarrow \partial \underline{\delta} / \partial \underline{a} = \underline{\Gamma}$:

$$\frac{\partial \underline{c}}{\partial \underline{a}} = \frac{\partial (\underline{\Gamma}^+ \underline{f})}{\partial \underline{a}} = \underline{\Gamma}^+ \frac{\partial \underline{f}}{\partial \underline{a}} = \underline{\Gamma}^+ \frac{\partial \underline{f}}{\partial \underline{\delta}} \frac{\partial \underline{\delta}}{\partial \underline{a}} = \underline{\Gamma}^+ \frac{\partial \underline{f}}{\partial \underline{\delta}} \underline{\Gamma}. \tag{28}$$

Here, the term

$$\frac{\partial \underline{f}}{\partial \underline{\delta}} = \underline{f}_{\underline{\delta}} = \text{diag} \left(\frac{\partial f}{\partial \delta}(t_0) \quad \frac{\partial f}{\partial \delta}(t_1) \quad \cdots \quad \frac{\partial f}{\partial \delta}(t_{N-2}) \quad \frac{\partial f}{\partial \delta}(t_{N-1}) \right) \tag{29}$$

means the instantaneous stiffness of nonlinear function of each sampling time per given cycle with resolution N [28]. As shown in Eq. (3), f_{δ} of dual stage stiffness $f_S(\delta)$ with $\alpha = 0$ only displays a vector string of zeros and ones according to the impact conditions. When nonlinear impact damping is added as Eq. (25), $f_S(\delta)\beta\dot{\delta}$ term affects f_{δ} , and instantaneous stiffness vector now includes elastic softening and spring back. Additionally, an arc-length continuation scheme based on excitation frequency ω_p [28–30], and a stability indicator using modified Hill’s method [34,35] are implemented in the HBM as used in this article. Refer to the companion paper [21] for more details. A comparison of the calculation efficiency between the semi-analytical method (HBM with $n_{\max} = 12$) and numerical simulation is also demonstrated in that work.

6. Nonlinear responses with impact damping alone

Typical nonlinear frequency response characteristics of impact damping, as expressed by Eq. (6), are studied first. Refer Table 2 for the relevant parameters and excitations. It should be noted that $\alpha = 1$ in $f_S(\delta)$ of Eq. (3) produces a linear stiffness. The viscous damping C of Eq. (2) is

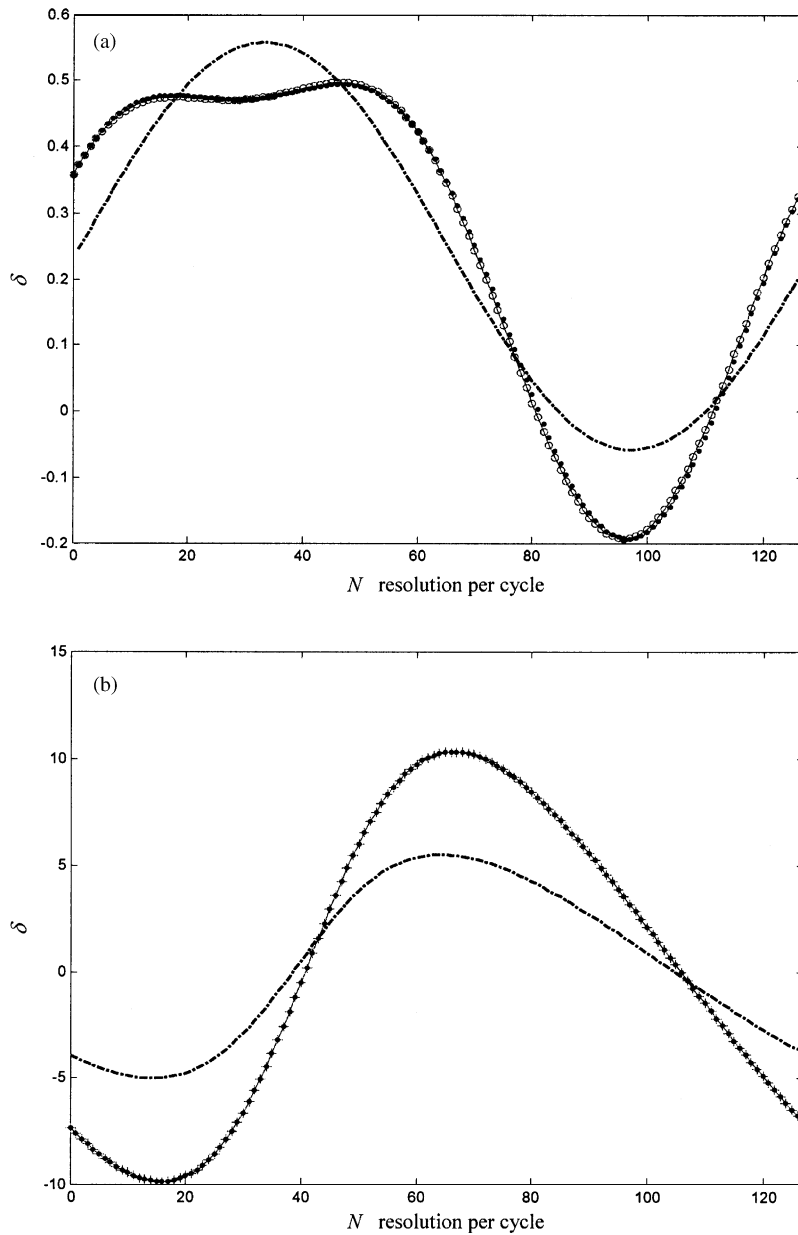


Fig. 4. Time history responses with impact damping alone with $\beta = 0.10$ (Case 1 of Table 2). (a) Super-harmonic response (at $\bar{Q} = 0.5$); and (b) primary harmonic response (at $\bar{Q} = 0.97$). Key: as in Fig. 3.

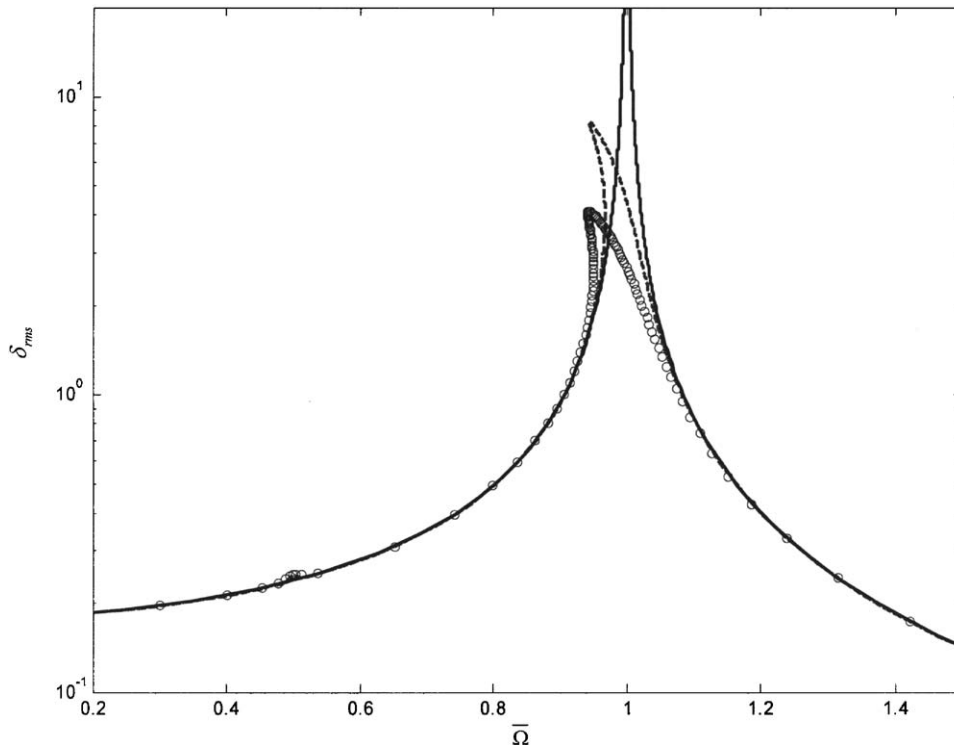


Fig. 5. Effect of β on primary harmonic and super-harmonic peaks for Case 1 of Table 2. All results are simulated by HBM with $n_{\max} = 12$. Key: —, $\beta = 0.00$; --, $\beta = 0.10$; and \circ , $\beta = 0.20$.

virtually zero so that its influence is negligible. Two cases of perturbation and mean torque ratios (F_p/F_m) are studied. The first ratio (Case 1) represents a condition when amplitude of F_p is about to exceed F_m . The $F_p/F_m \geq 1$ condition typically triggers significant nonlinear responses including super- and sub-harmonics and unstable conditions in the clearance-type nonlinearity [8,12,13,19–21]. Such tendencies are also observed in the impact damping case as seen in Figs. 3–5. Here, the non-dimensionalized frequency $\bar{\Omega}$ is defined as $\bar{\Omega} = \omega_p/\omega_r$. The responses in Figs. 3 and 5 are given in terms of the maximum or rms value of relative displacement $\delta(t)$. Here, the δ value is presented on a log scale to magnify the super-harmonic responses at $\bar{\Omega} = 0.5$, and to compare the effect of damping at $\bar{\Omega} = 0.1$. Fig. 4 shows time domain response with N resolutions per cycle.

First, the frequency response results from various semi-analytical methods are correlated in Fig. 3 to that yielded by the numerical integration (NS). Both down (NSD) and up (NSU) frequency are needed in numerical simulation to acquire the nonlinear frequency shift around the resonance $\bar{\Omega} = 1.0$. The super-harmonic response at $\bar{\Omega} = 0.5$ is clearly simulated by NS. This super-harmonic peak is related to the $\sin(\Phi_p) \cos(\Phi_p)$ component of the nonlinear Eq. (6) that can be expressed with $\sin(2\Phi_p)$. As seen in Fig. 3, multi-harmonic HBM (with $n_{\max} = 12$) can simulate the frequency shift around the resonance as well as the super-harmonic response like NS. With a single frequency sweep, HBM can also adjust its frequency step size to suit the Newton–Raphson

convergence criteria, and provides the solution stability results. Typical HBM results of the frequency shift around $\bar{\Omega} = 1.0$ indicate some unstable solutions, as evident from the time history of Fig. 4(a). Even though these solutions are unstable, HBM yields a periodic time history in contrast with the quasi-periodic results from NS. For the super-harmonic response, time histories from HBM and NS match well since the response stays periodic as seen in Fig. 4(b). Both DFM and SLM methods can also simulate this frequency shift around the resonance with reasonable accuracy as evident from Fig. 4(b), but not the super-harmonic response. This is because they rely only on the fundamental harmonic. However, both DFM and SLM are better tools for a weakly nonlinear system since they provide analytical solutions. They also yield an improved understanding of the underlying physical effects.

The effect of the impact damping is studied by varying β from 0.0 to 0.2 using the multi-harmonic HBM, and nonlinear responses are shown in Fig. 5. When β assumes a larger value, the extent of nonlinearity increases. The peak amplitude around $\bar{\Omega} = 1.0$ decreases as β increases, and the frequency shift around $\bar{\Omega} = 1.0$ follows the same tendency. This may be thought of as a “damped” natural frequency of the system $\omega_{rd} = \sqrt{1 - 2\zeta^2}\omega_r$ where ω_r is affected by the impact

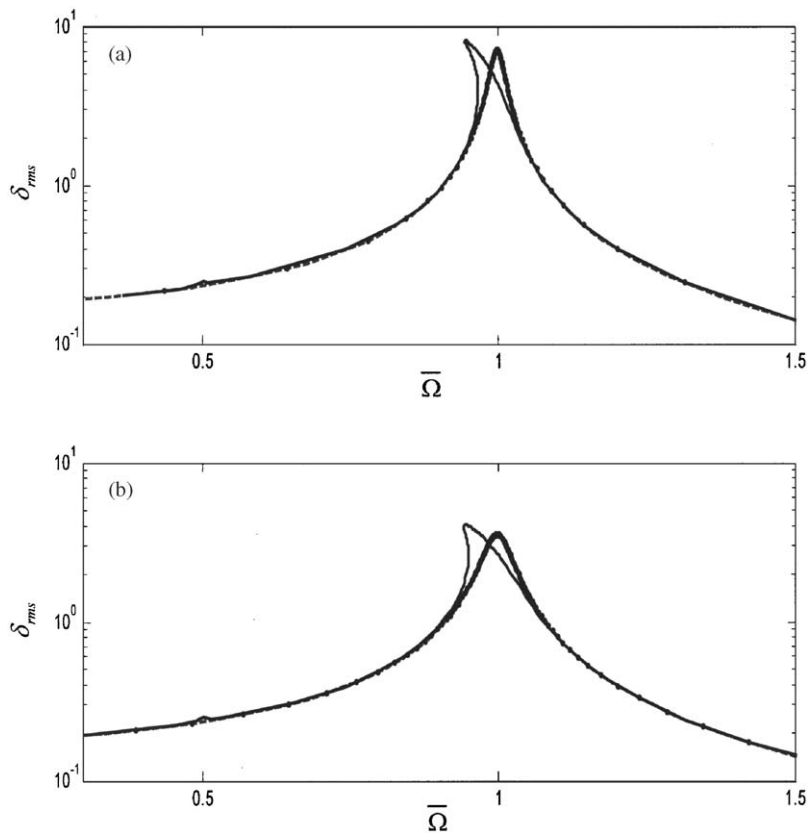


Fig. 6. Comparison of nonlinear responses with impact damping as simulated by DFM, HBM and SLM (with effective viscous damping) methods for Case 1 of Table 2. (a) $\beta = 0.10$; (b) $\beta = 0.20$. Key: —, HBM; --, DFM; and ●, SLM.

damping-related term $\sqrt{1 - 2\zeta^2}$, but not by the stiffness-related $\omega_r = \sqrt{K/I}$ term. Such effects can also be predicted using other semi-analytical methods like DFM and SLM with reasonable accuracy as shown in Fig. 6. When comparing with HBM, both DFM and SLM provide faster and simpler predictions of the impact damping effect at and near the resonance. Based on SLM, the effective but spectrally varying viscous damping (\bar{C}) and effective stiffness (\bar{K}) values are calculated using Eqs. (19c) and (19d). The effective stiffness of the system stays as unity as predicted by Eq. (21). Only \bar{C} changes when β is varied. Fig. 7(a) shows \bar{C} values as calculated by SLM when β is varied from 0.05 to 0.2. Fig. 7(b) clearly indicates a significant drop in \bar{C} near the fundamental harmonic and super-harmonic resonances, as calculated by HBM. However, \bar{C} results as calculated by SLM cannot reproduce the nonlinear characteristics when the nonlinear impact damping is replaced by an equivalent viscous damping as seen earlier in Fig. 6. Such results fail to simulate both the amplitude changes and frequency shifts included by the impact damping. From the observations stated above, the unstable frequency response regime around $\bar{\Omega} = 1.0$ and a small super-harmonic response at $\bar{\Omega} = 0.5$ constitute the unique nonlinear response characteristics corresponding to the impact damping nonlinearity itself. The spectrally invariant viscous damping could be viewed as the proper model except near $\bar{\Omega} = 1.0$ and 0.5 since such resonance regimes produce a significant drop in \bar{C} values.

The same phenomena and responses are observed for Case 2 of Table 2. This represents a condition that has a large mean torque but small perturbations. As seen in Fig. 8, the ratio

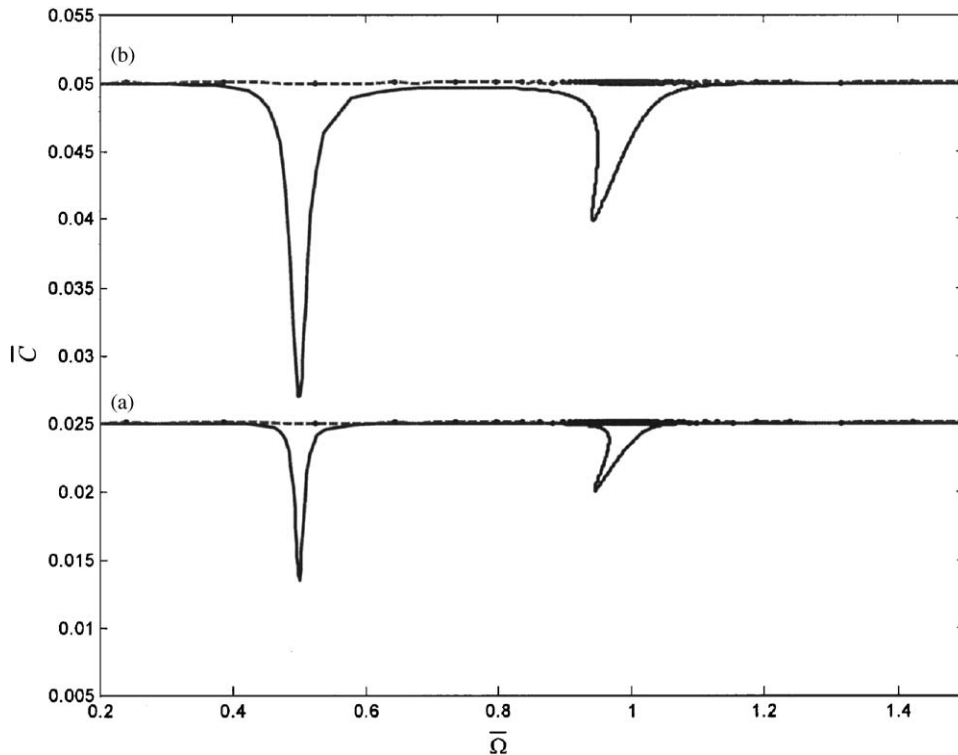


Fig. 7. Effective viscous damping values for the impact damping alone (Case 1 of Table 2). (a) $\beta = 0.10$; and (b) $\beta = 0.20$. Key: as in Fig. 6.

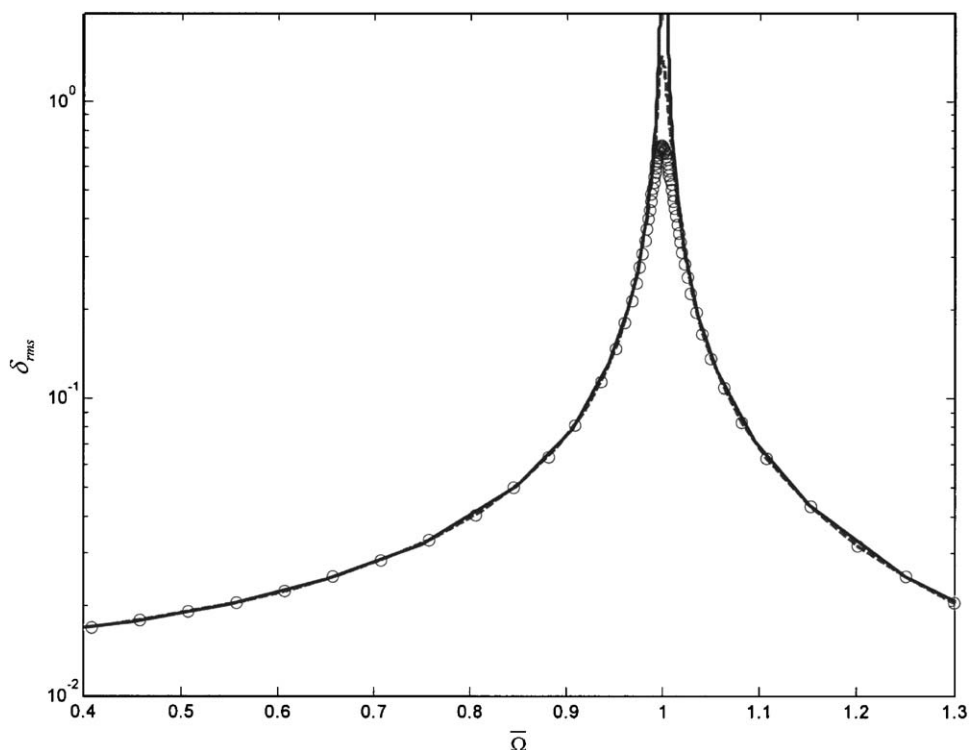


Fig. 8. Effect of β on primary harmonic peaks for Case 2 of Table 2. All results are simulated using HBM with $n_{\max} = 12$. Key: —, $\beta = 0.00$; --, $\beta = 0.10$; and \circ , $\beta = 0.20$.

$F_p/F_m = 0.2$ does not show any unstable solution regime around the resonance peak. But the frequency shifts and amplitude reductions can still be found. The super-harmonic response at $\bar{\Omega} = 0.5$ is also observed, but with a very small amplitude. The \bar{C} values as calculated by HBM show in Fig. 9 some reductions in resonant and super-harmonic response peaks, but not as much as those seen in Fig. 7 for the higher torque perturbation case. This shows that the F_p/F_m ratio affects the reliability of predictions when DFM or SLM is used. Lower F_p/F_m ratios yield good predictions, as evident from a comparison of results between Figs. 6 and 10. When the \bar{C} value is substituted in a linear model as the overall viscous damping, the amplitude of response matches solutions from the nonlinear damping model, but the frequency shift cannot be simulated.

7. Effect of impact damping and clearance nonlinearities

The effect of combined nonlinearities is studied next with focus on super- and sub-harmonic responses. Figs. 11 and 12 show results for Case 3 of Table 2. The $\delta_{rms}(\bar{\Omega})$ curves as calculated by HBM and NS are compared in Fig. 11 for $\beta = 0.02$ and 0.04. The sub-harmonic response curve exhibits a clear separation from the main frequency response in Fig. 11(b). As seen in Fig. 12, the

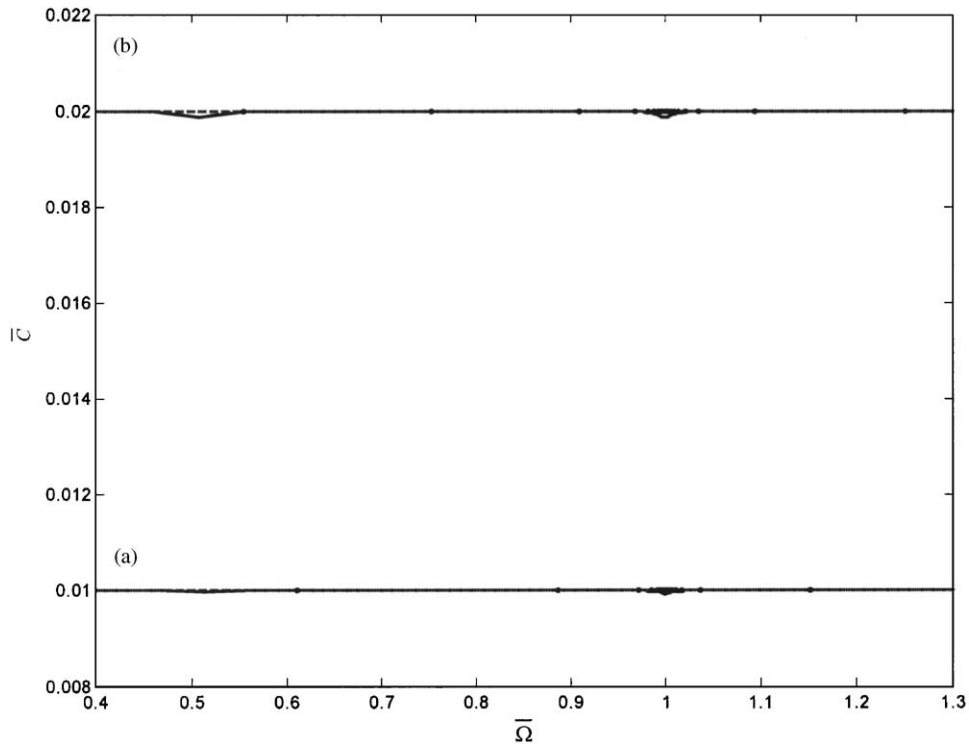


Fig. 9. Effective viscous damping values for Case 2 of Table 2. (a) $\beta = 0.10$; and (b) $\beta = 0.20$. Key: as in Fig. 6.

separation (ℓ in $\bar{\Omega}$ units) between the fundamental harmonic resonance ($\bar{\Omega}_{p1}$) to the mean point (δ_m) intersection is not affected by the impact damping. Therefore, the existence of sub-harmonic remains the same as we found earlier from a pure clearance nonlinearity [8,12,13,19–21]. The unstable solution regime associated with the sub-harmonic response diminishes when β is increased as seen in Fig. 11. Similar reductions of the unstable solution regime are also observed at the tip of sub-harmonic response, on quasi-periodic responses at $\bar{\Omega} = 0.53$ and 0.38 , and at the super-harmonic peaks. Thus the impact damping adds more damping and tends to stabilize the system. Numerical results from NS as shown in Figs. 11(a) and (b) validate such observations.

The effect of impact damping on super-harmonics is illustrated in Fig. 13. Using the parameters of Case 4 of Table 2, super-harmonic peaks ($\bar{\Omega}_p/2$, $\bar{\Omega}_p/3$ and $\bar{\Omega}_p/4$) are predicted using the HBM. Even when β is as high as 0.4, all the super-harmonic peaks still exist, though their amplitudes diminish slightly. In Fig. 14(a,b), the spectrally varying effective \bar{C} (from impact damping alone) and \bar{K} (from the clearance nonlinearity alone) spectra are presented. The effective stiffness \bar{K} based on DFM cannot predict a decrease in the first stage of the multi-staged stiffness function $f_S(\delta)$, but the multi-harmonic SLM and HBM simulate such characteristics. The effective damping \bar{C} values match with our simple prediction based on Eq. (6) for the linear stiffness

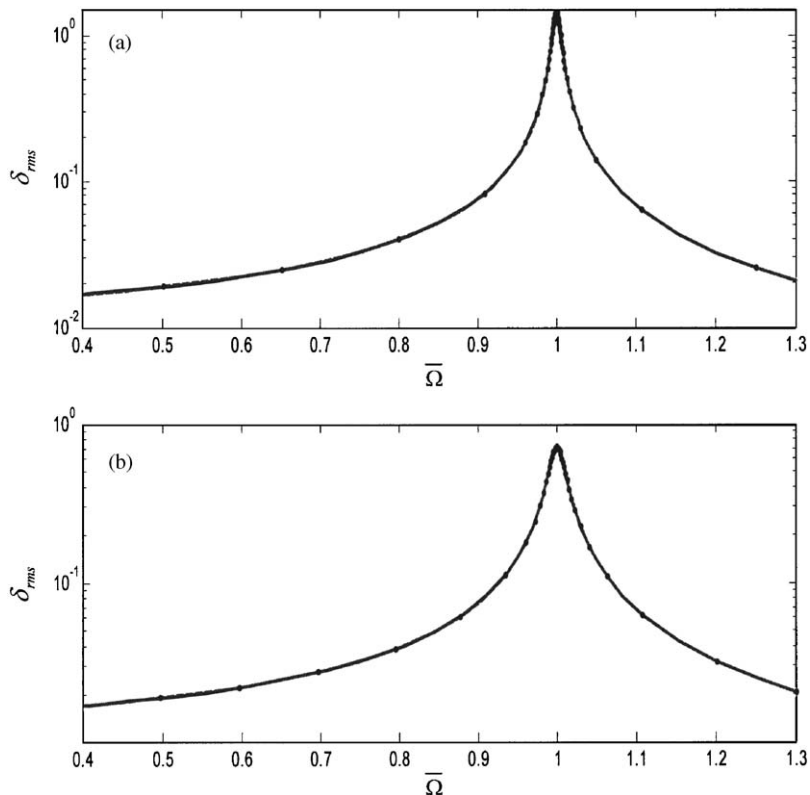


Fig. 10. Comparison of nonlinear responses with impact damping as simulated using DFM, HBM and SLM (with effective viscous damping) methods for Case 2 of Table 2. (a) $\beta = 0.10$; and (b) $\beta = 0.20$. Key: as in Fig. 6.

regime. But additional damping is found when the stiffness transition occurs. Only the multi-harmonic semi-analytical methods such as HBM can simulate the \bar{C} values in the super-harmonic regime.

Based on the results and observations stated above, it seems that the multi-staged stiffness nonlinearity $f_S(\delta)$ governs the overall shape of frequency response curve, and as expected the nonlinear impact damping affects the resonant and super- and sub-harmonic responses. The impact damping does not affect the appearance of super-harmonics, rather it controls their amplitudes. Finally, the impact damping may alter the sub-harmonic system response since it tends to provide some stability.

8. Conclusion

Chief contribution of this article is the development of frequency response characteristics of the nonlinear impact damping, without and with the influence of clearance-type nonlinearity.

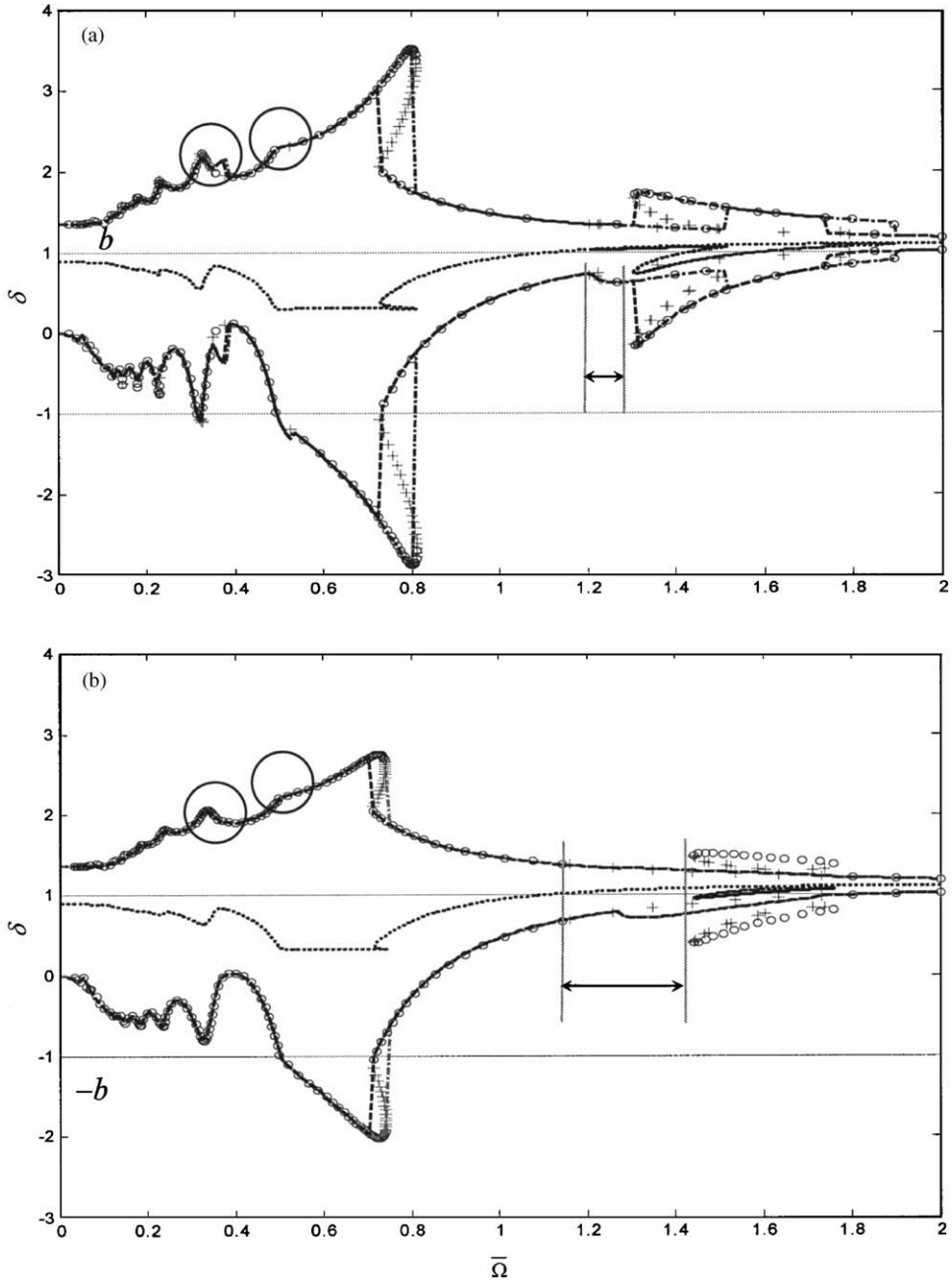


Fig. 11. Comparison between numerical simulation (NS) and multi-harmonic HBM results for clearance and impact damping nonlinearities (Case 3 of Table 2 given $\alpha = 0.15$). (a) $\beta = 0.20$; (b) $\beta = 0.40$; Key: \circ , HBM stable ($n_{\max} = 12$); $+$, HBM unstable ($n_{\max} = 12$); $- \cdot -$, NSU; $- \cdot -$, NSD; and \dots , δ_m .

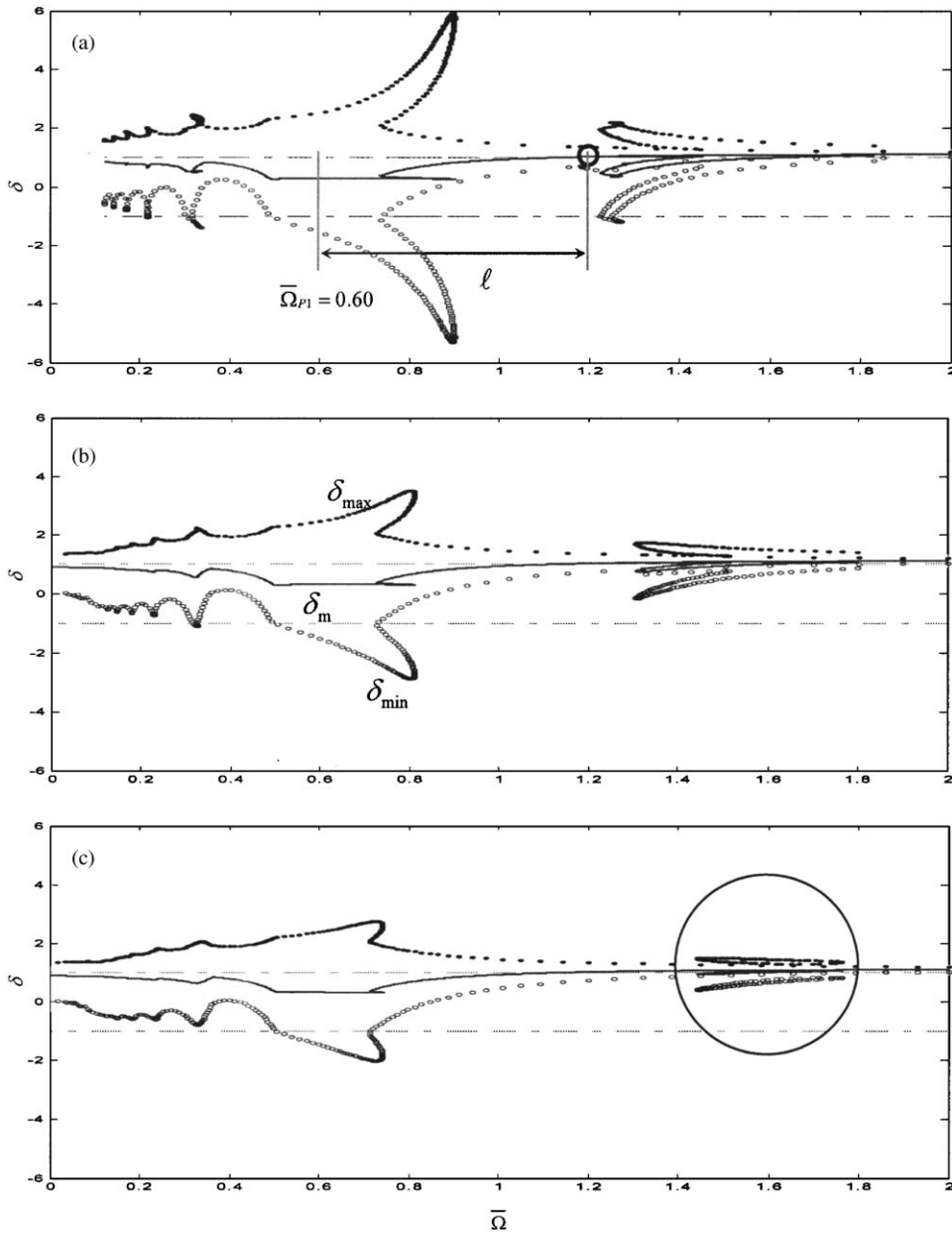


Fig. 12. Super- and sub-harmonic appearances related to clearance and impact damping nonlinearities for Case 3 of Table 2 with $\alpha = 0.15$. (a) $\beta = 0.00$; (b) $\beta = 0.20$; and (c) $\beta = 0.40$. Key: $-$, δ_m ; \cdot , δ_{max} ; \circ , δ_{min} ; $- \cdot$, $\pm b$.

Semi-analytical methods like HBM, DFM, and SLM can predict the effective viscous damping value arising from the nonlinear damping mechanism, especially when the F_p/F_m ratio is small. This implies that the nonlinear impact damping is more affected by the dynamic

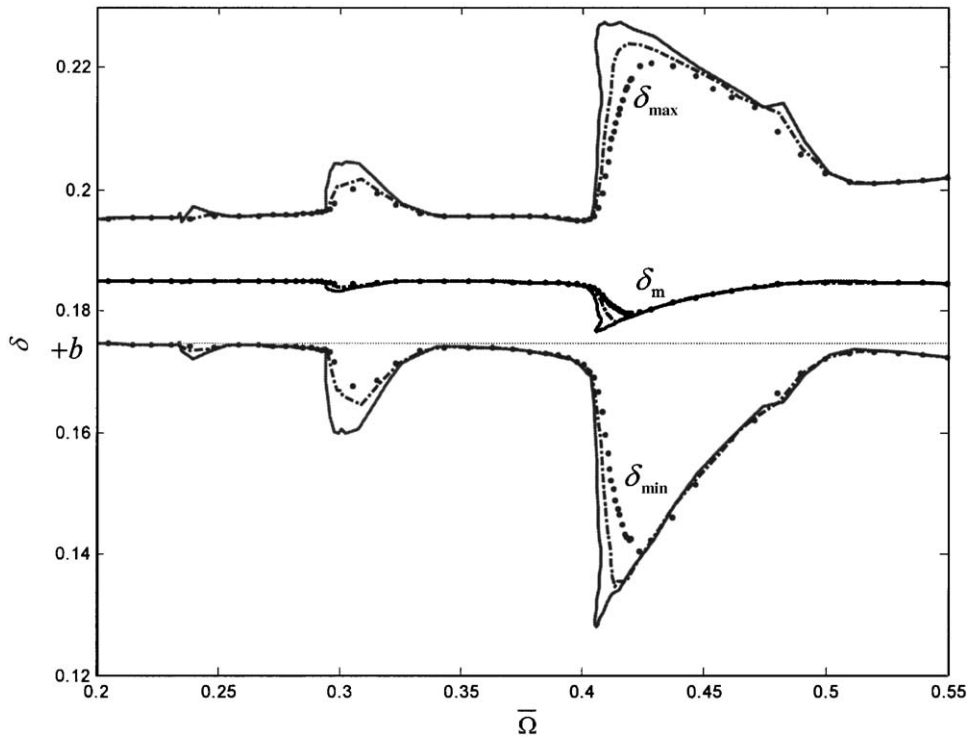


Fig. 13. Super-harmonic responses produced by clearance and impact damping nonlinearities (Case 4 of Table 2 with $F_p/F_m = 0.185$). Key: —, $\beta = 0.00$; - - , $\beta = 0.20$; and · · · , $\beta = 0.40$.

torque input. The impact damping reduces the peak resonant amplitudes, enhances dynamic stability and reduces quasi-periodic or chaotic regimes, while introducing a small frequency shift. The impact damping effects in a practical automotive driveline system may seem to be small, but it controls the peak-to-peak acceleration levels. Consequently, one must include impact damping elements in vibro-impact simulation codes. In a recent study [36], vibration of a double sphere-plane pre-loaded system with Hertzian dry element and under a pure harmonic force was examined. The authors of this study also recommend further research to determine the precise mechanisms of damping under vibro-impact conditions.

Acknowledgements

This project has been supported by the Gear Rattle Industrial Consortium (Eaton R&D, Spicer Clutch, CRF Fiat, Luk, SAAB and Volvo Trucks) over the 1998–2000 period, and the DaimlerChrysler Challenge Fund from 2000 to 2003.

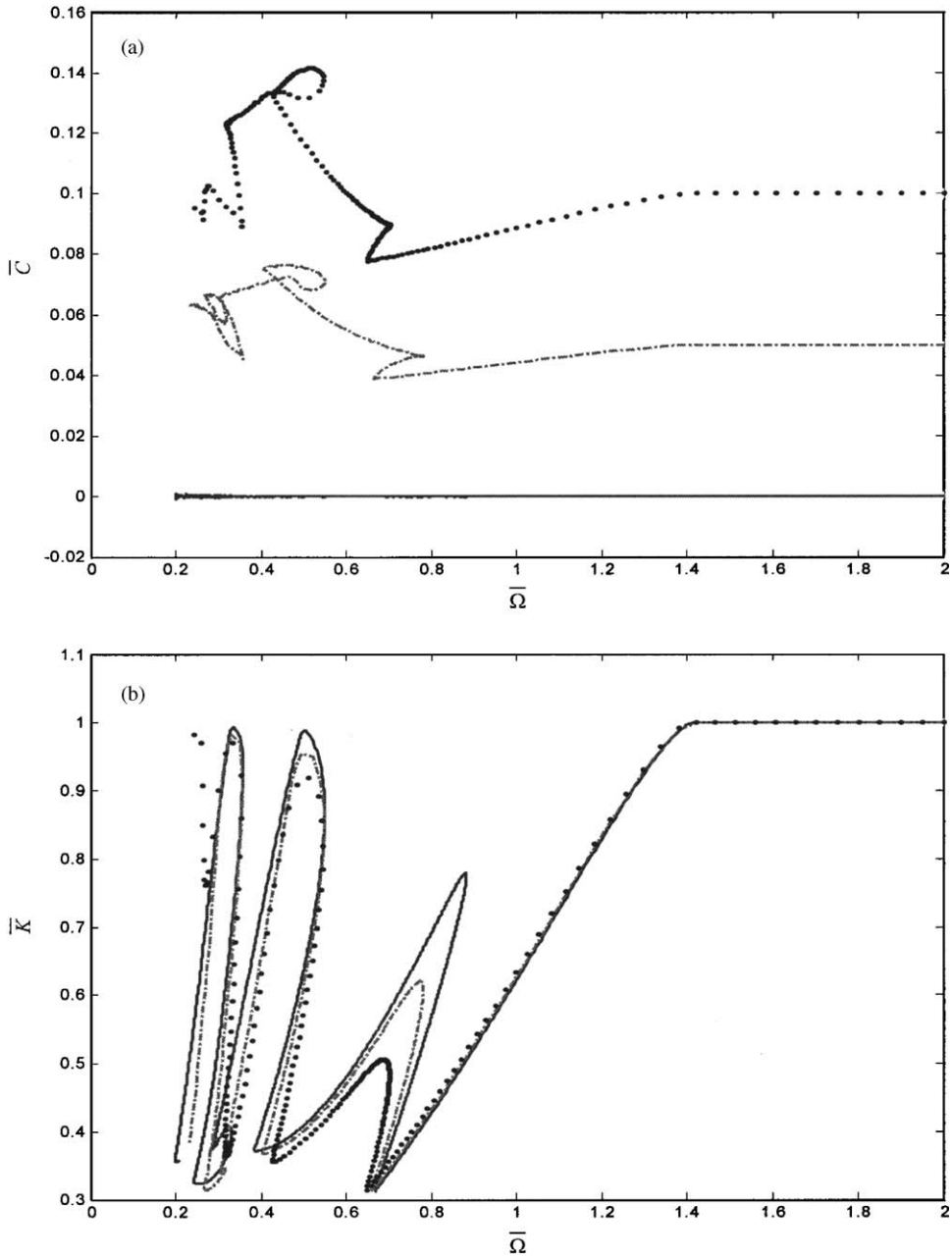


Fig. 14. Effective (a) viscous damping, and (b) stiffness spectra for Case 4 of Table 2 with $\alpha = 0.0$ (HBM with $n_{\max} = 12$). Key: —, $\beta = 0.00$; - ·, $\beta = 0.10$; and ·, $\beta = 0.20$.

References

- [1] K.H. Hunt, F.R.E. Crossley, Coefficient of restitution interpreted as damping in vibro-impact, *Journal of Applied Mechanics* 42 (1975) 440–445.
- [2] S. Dubowsky, F. Freudenstein, Dynamic analysis of mechanical systems with clearances, Part 1: formation of dynamic model, *Journal of Engineering for Industry* 93 (1971) 305–309.
- [3] S. Dubowsky, F. Freudenstein, Dynamic analysis of mechanical systems with clearances, Part 2: dynamic response, *Journal of Engineering for Industry* 93 (1971) 310–316.
- [4] M.A. Veluswami, F.R.E. Crossley, Multiple impacts of a ball between two plates, Part 1: some experimental observations, *Journal of Engineering for Industry* 97 (1975) 820–827.
- [5] M.A. Veluswami, F.R.E. Crossley, Multiple impacts of a ball between two plates, Part 2: some mathematical modeling, *Journal of Engineering for Industry* 97 (1975) 828–835.
- [6] R.C. Azar, F.R.E. Crossley, Digital simulation of impact phenomenon in spur gear systems, *Journal of Engineering for Industry* 99 (1977) 792–798.
- [7] D.C.H. Yang, J.Y. Lin, Hertzian damping, tooth friction and bending elasticity in gear impact dynamics, *Journal of Mechanisms, Transmissions, and Automation in Design* 109 (1987) 189–196.
- [8] C. Padmanabhan, R. Singh, Dynamics of a piecewise non-linear system subject to dual harmonic excitation using parametric continuation, *Journal of Sound and Vibration* 184 (5) (1995) 767–799.
- [9] R.G. Herbert, D.C. McWhannell, Shape and frequency composition of pulses from an impact pair, *Journal of Engineering for Industry* 99 (1977) 513–518.
- [10] J. Shaw, S.W. Shaw, The onset of chaos in a two-degree-of-freedom impacting system, *Journal of Applied Mechanics* 56 (1989) 168–174.
- [11] R. Singh, H. Xie, R.J. Comparin, Analysis of an automotive neutral gear rattle, *Journal of Sound and Vibration* 131 (1989) 177–196.
- [12] R.J. Comparin, R. Singh, Non-linear frequency response characteristics of an impact pair, *Journal of Sound and Vibration* 134 (2) (1989) 259–290.
- [13] R.J. Comparin, R. Singh, An analytical study of automotive neutral gear rattle, *Journal of Mechanical Design* 112 (1990) 237–245.
- [14] R.J. Comparin, R. Singh, Frequency response of multi-degree of freedom system with clearances, *Journal of Sound and Vibration* 142 (1990) 101–124.
- [15] F. Pfeiffer, A. Kunert, Rattling models from deterministic to stochastic processes, *Nonlinear Dynamics* 1 (1990) 63–74.
- [16] K. Karagiannis, F. Pfeiffer, Theoretical and experimental investigations of gear-rattling, *Nonlinear Dynamics* 2 (1991) 367–387.
- [17] M. Kataoka, S. Ohno, T. Sugimoto, A two-degree-of-freedom system including a clearance two-step hardening spring, *Japan Society of Mechanical Engineers, International Journal Series II* 34 (1991) 345–354.
- [18] C. Padmanabhan, R.C. Barlow, T.E. Rook, R. Singh, Computational issues associated with gear rattle analysis, *Journal of Mechanical Design* 117 (1995) 185–192.
- [19] T.E. Rook, R. Singh, Dynamic analysis of a reverse-idler gear pair with concurrent clearances, *Journal of Sound and Vibration* 182 (2) (1995) 303–322.
- [20] T.C. Kim, T.E. Rook, R. Singh, Effect of smoothening functions on the frequency response of an oscillator with clearance non-linearity, *Journal of Sound and Vibration* 263 (2003) 665–678.
- [21] T.C. Kim, T.E. Rook, R. Singh, Super- and sub-harmonic response calculations for a torsional system with clearance non-linearity using the harmonic balance method, *Journal of Sound and Vibration* 281, (3–5) (2005) 965–993, this issue, doi:10.1016/j.jsv.2004.02.039.
- [22] Y. Chikatani, A. Suehiro, Reduction of ideling rattle noise in trucks, SAE Paper No. 911044, 1991, pp. 49–56.
- [23] T.C. Kim, R. Singh, Dynamic interactions between loaded and unloaded gear pairs under rattle conditions (Paper no. 2001-01-1553), *SAE Transactions, Journal of Passenger Cars: Mechanical Systems* 110(Section 6) (2001) 1934–1943.
- [24] R. Seydel, *Practical Bifurcation and Stability Analysis*, Springer, Berlin, 1994.

- [25] A. Gelb, W.E. Vander Velde, *Multiple-Input Describing Functions and Non-linear System Design*, McGraw-Hill, New York, 1968.
- [26] J.R. Dormand, P.J. Prince, New Runge–Kutta algorithms for numerical simulation in dynamical astronomy, *Celestial Mechanics* 18 (1978) 223–232.
- [27] J. Wallascheck, Dynamics of non-linear automobile shock-absorbers, *International Journal of Non-linear Mechanics* 25 (1990) 299–308.
- [28] G. von Groll, D.J. Ewins, The harmonic balance method with arc-length continuation in rotor/stator contact problems, *Journal of Sound and Vibration* 241 (2) (2001) 223–233.
- [29] E.L. Allgower, K. Georg, *Numerical Continuation Methods: An Introduction*, Springer, New York, 1990.
- [30] P. Sundararajan, S.T. Noah, Dynamics of forced nonlinear systems using shooting/arclength continuation method—application to rotor systems, *Journal of Vibration and Acoustics* 119 (1997) 9–20.
- [31] R. Gasch, K. Knothe, *Strukturdynamik II*, Springer, Berlin, 1989.
- [32] G. Genta, *Vibration of Structures and Machines*, third ed, Springer, Berlin, 1999.
- [33] F.H. Ling, X.X. Wu, Fast Galerkin method and its application to determine periodic solutions of non-linear oscillations, *International Journal of Non-linear Mechanics* 22 (1987) 89–98.
- [34] P. Sundararajan, S.T. Noah, An algorithm for response and stability of large order non-linear systems, application to rotor systems, *Journal of Sound and Vibration* 214 (1998) 695–723.
- [35] G. von Groll, D.J. Ewins, On the dynamics of windmilling in aero-engines, *The 6th International Conference on Vibrations in Rotating Machinery UK*, Institution of Mechanical Engineers, 2000.
- [36] E. Rigaud, J. Perret-Liaudet, Experiments and numerical results on non-linear vibrations of an impacting Hertzian contact. Part I: harmonic excitation, *Journal of Sound and Vibration* 265 (2) (2003) 309–327.